


Enhancement of microcantilever beams fabrication and determination of their mechanical properties using nanoindentation

Yung-Chiang Chung , Cheng-Feng Lin

Department of Mechanical Engineering, Ming Chi University of Technology, 84, Gung- Juan Road, Taishan, New Taipei, Taiwan

✉ E-mail: ycchung@mail.mcut.edu.tw

Published in Micro & Nano Letters; Received on 11th October 2018; Revised on 3rd January 2019; Accepted on 27th February 2019

Microcantilever beams were fabricated through a microelectromechanical system fabrication process; this process was improved by using etched slots. The actual mechanical properties of the cantilever beams can be estimated using a nanoindenter. Various cantilever beam widths and length-to-width ratios were used for evaluation. Five structures of cantilever beams were fabricated and compared. ANSYS software was used to simulate cantilever beam deflections. The etched slots increased the cantilever beam deflections, and the increase in deflection was apparent when the etched slot was located near the base of the beams. Type 4 was a cantilever beam with an etched slot of length $L/2$ near the base of the beam. The area of the etched slots of type 4 was larger, and the etched slot of type 4 was near the base of the cantilever beam. Type 4 had the shortest etching time, highest fabrication success rate, and greatest deflection. The difference between the measured and simulated (without parameter modification) deflections could exceed 10%. Modifying the force acting point and Young's modulus in the simulations reduced the difference between the measured and simulated deflections to 0.5%. This demonstrates that actual experimental conditions considerably influence simulation results, and this can be beneficial to subsequent studies.

1. Introduction: Microcantilever beams are widely used for many applications, and microcantilever beam fabrication methods have also been discussed by many researchers [1, 2]. The reliability of a microcantilever beam is an important issue before the device can be used. It is indispensable to study the success rate, etching time, and deflection of the microcantilever beam fabrication. However, the researches of investigating these parameters are less. Researchers in a previous study applied the MAT-Test technique and MFT2000 system to measure Young's modulus and stress of a material [3]. However, this technique has a disadvantage in that the stylus utilised could slip easily when the deflection of the cantilever beam is large. In another study, the deflection of cantilever arrays was measured by considering polymer film expansion and contraction, and the elastic property was also varied [4]. Moreover, an audible frequency generator was designed and fabricated in a study by using an electrostatic microcantilever array [5]. Another study discussed microcantilever vibration under thermal base excitation [6]. Numerous studies have applied the nanoindentation technique for measuring the mechanical properties of a material [7, 8]. The nanoindentation technique has also been used in various applications such as in determining mechanical stability [9], load-strain rates [10], plastic deformation [11], loading-unloading curves for various cycles at varying forces [12], deformation behaviour of two-phase amorphous alloys [13], high-temperature nanomechanical properties [14], viscoplastic behaviour [15], photo-induced mechanical properties [16], hydrogen effects on mechanical properties [17], and nanomechanical properties of dendrimers coated on a titanium surface [18]. Furthermore, a study reviewed the nanoindentation measurement technique [19], and other studies have applied this technique to determine the micromechanical properties of microcapsules [20] and the mechanical properties of an SU-8 photoresist (PR) [21]. In particular, the technique has been applied to determine the viscoelastic behaviour of human tooth enamel [22], nanoindentation and tensile modulus of plant cell walls [23], and deformation behaviour of an insect [24]. The mechanical properties of microstructures are crucial for the acceleration of fabrication processes. However, the properties of macroscale structures cannot be directly used in micro- and nano-scale structures. The properties of micro-

nano-structures usually depend on the fabrication process; therefore, the actual properties of these structures should be measured. For example, the values of Young's modulus are in a large range (52.5–370 GPa) that depend on the fabrication processes and researches [25]. The nanoindentation technique is often used and is simple, rapid, and accurate. The applications of the microcantilever beams included the electrical switch [26], accelerometer [27], sensors of temperature [28], viscosity [29], calorimetry [30], clinical biochemical [31], protein [32], DNA [33], and cancer diagnosis [34]. The applications of the microcantilever beams were comprehensive. The etching process is a crucial step in the fabrication of microcantilever beams; however, the etching time is long, thus constituting a bottleneck in fabrication processes. Therefore, reducing the etching time is imperative. The current study proposes a method for reducing the etching time and increasing the success rate of fabricating microcantilever beams, for deriving the exact Young's modulus and deflection of beams through the nanoindentation technique, and for the deflection difference between experimental fabrication and simulation. However, the time of the microcantilever beams fabrication was long, and the success rate of the microcantilever beams fabrication was not high. When the microcantilever beams were used to be the sensor, the deflection was related to the sensitivity, especially in biology. The deflection was larger, and the sensitivity was higher, too. It is valuable for reducing the etching time, increasing the success rate and deflection. The time of fabrication, success rate, and deflection of the microcantilever beams were important, and these parameters will be discussed in this study.

2. Material and methods

2.1. Principle of operation: When a force is exerted on a microcantilever beam, the displacement that occurs at some point of the beam is known as deflection. Based on theorems and derivations [35], the length of the cantilever beam is L , the fixed end of the cantilever beam is the original point, and the x -axis runs along the length of the cantilever beam. The force (or load) P is exerted on the free end of the cantilever beam, and the deflection $v(x)$ of a position x

on the cantilever beam can be expressed as

$$v(x) = \frac{Px^2(3L-x)}{6EI} \quad 0 \leq x \leq L \quad (1)$$

where E is Young's modulus and I is the moment of inertia. When $x = L$ (free end), the maximum deflection of the cantilever beam can be expressed as

$$v_{\max} = v(L) = \frac{PL^3}{3EI} \quad (2)$$

2.2. Chip design and fabrication: Five types (types 1–5) of cantilever beams are displayed in Fig. 1. A silicon wafer with a silicon nitride film (MUSTC CORP., Taiwan, R.O.C.) was used in this study. The etchant was buffered oxide etchant (BOE, with the main species including hydrofluoric acid and ammonium fluoride). The silicon wafer with the silicon nitride film was fabricated through bulk micromachining. The fabrication process is presented in Fig. 2. First, the wafer was cleaned with acetone, and the

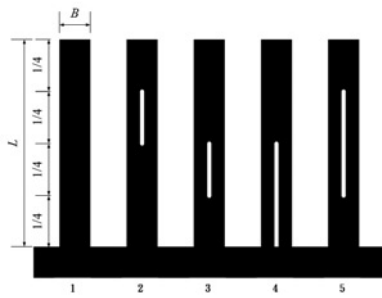


Fig. 1 Schematic diagram of the five types of cantilever beams

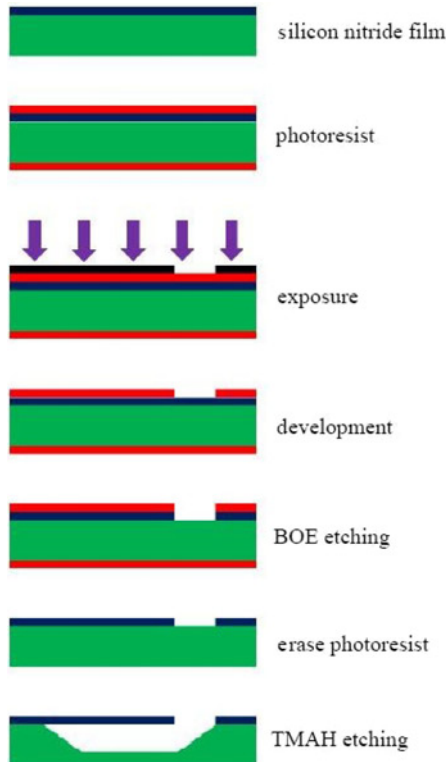


Fig. 2 Schematic drawings of the fabrication process of cantilever beams

remaining acetone on the wafer surface was removed using isopropanol. Subsequently, the water on the surface of the wafer was removed using a heated plate. Hexamethyldisilazane was added to improve adhesion, and a photoresist (PR, type AZ-5214E) measuring $1\ \mu\text{m}$ was prepared on the surface of the wafer by using a spin coating. The wafer was baked at 95°C (soft bake) to extract the solvent from the PR, thus appropriately exposing the PR. The PR was exposed to an ultraviolet light source to determine the pattern. The wafer was baked at 100°C after exposure to again extract the solvent from the PR. Moreover, the regions that were not protected by the mask on the wafer surface were removed by a developer (AZ-300MIF). The wafer was baked at 105°C (hard bake) to improve the adhesion of the PR and increase the etch resistance of the PR. BOE was used to erase the silicon nitride without any protection. The PR was cleaned with acetone, and the acetone on the wafer surface was removed using isopropanol. Finally, the wafer was cleaned with deionised (DI) water. Moreover, tetramethylammonium hydroxide (25%) and a stirrer (200 rpm) were used to etch the silicon nitride on the surface of the wafer at 95°C ; the etching rate was $\sim 80\ \mu\text{m/h}$. After etching, the wafer was soaked in DI water and then soaked in alcohol to clean the wafer. The wafer was baked at 120°C to evaporate the alcohol. Subsequently, the wafer was observed under a microscope, and the size of each fabricated microcantilever beam was measured.

The appearance and size of the beams were observed and measured using an optical microscope (CKX41, Olympus, Japan). Young's modulus and deflection were measured using a nanoindenter (TI 950 TriboIndenter, Hysitron, USA) equipped with a Berkovich 142.3° diamond probe tip. Five indentation tests were performed for each sample. The Young's modulus of each sample was determined based on the Oliver and Pharr method [36, 37]. The Young's modulus, E , was expressed as follows:

$$\frac{1}{E_r} = \frac{1 - \nu^2}{E} + \frac{1 - \nu_i^2}{E_i} \quad (3)$$

where E , ν , E_i and ν_i are Young's modulus and Poisson's ratio of the tested material and diamond indenter, respectively. E_r is the reduced Young's modulus

$$E_r = \frac{\sqrt{\pi}}{2} \frac{S}{\sqrt{A}} \quad (4)$$

where S is the stiffness of the specimen, A is the projected contact area of indentation. In this work, Young's modulus and Poisson's ratio of the diamond indenter are 1140 GPa and 0.07, respectively, whereas the Poisson's ratio of the Si_3N_4 material is 0.25 [25].

3. Numerical simulation: Before the chips were fabricated, deflection simulations were conducted for the five types of microcantilever beams. The results can facilitate the determination of the maximum deflection and reduce the fabrication time and cost. The simulations were based on the finite volume method and three-dimensional structured grids as implemented in the ANSYS software package (Swanson Analysis Systems, Inc., Pennsylvania, U.S.A.). The total number of elements were about 4000. The boundary condition was set to be fixed at the bottom. The simulations were performed using the mechanical solver. The material properties were provided by ANSYS. The five microcantilever beams (Fig. 1) were compared to determine the differences in deflection. Type 1 did not have an etched slot, and types 2–5 had one etched slot each. Types 2 and 3 had an etched slot length of $L/4$, where L is the total length of the cantilever beam; however, the locations of the slots differed. The etched slot length of types 4 and 5 was $L/2$; however, the locations of the slots also differed. The widths of the cantilever beams were 50, 100, 150, and $200\ \mu\text{m}$, respectively, and the length-to-width ratios ranged from 1 to 5. For example, the

lengths of the cantilever beams with width 50 μm were 50, 100, 150, 200, and 250 μm , respectively. The lengths of the cantilever beams with width 200 μm were 200, 400, 600, 800, and 1000 μm , respectively. The thickness of each cantilever beam was 1 μm , the width of etched slots was 10 μm , and the force (load) exerted at the free end was 200 μN . The width of the etched slots was kept constant in various widths of the beam. The material used was silicon nitride, and the value of Young's modulus was 142 GPa.

4. Results and discussion: This study analysed the effects of etched slots on the etching time, success rate, and deflection during the fabrication of microcantilever beams. Moreover, the relationship between the deflection and force was examined using the nanoindentation technique, and the value of Young's modulus during simulation was analysed to determine its precision. Each set of experimental conditions was repeated at least four times, with the average error being less than 20%.

4.1. Simulation results: The simulated deflections of type 1 at a width of 200 μm , various lengths, and a free-end force of 200 μN are illustrated in Figs. 3a–e. The deflections increased with the length-to-width ratios when the width remained constant. The simulation results for type 2 at various lengths are presented in Figs. 4a–e, and those for type 4 are presented in Figs. 5a–e. The tendency of types 2–5 beams was similar to that of type 1 (figures of types 3 and 5 are not shown). The deflections of types 1–5 with various widths during simulation are shown in Figs. 6a–d. The deflections of types 1–5 increased by increasing the length/width ratios. When the width was 100 μm , the

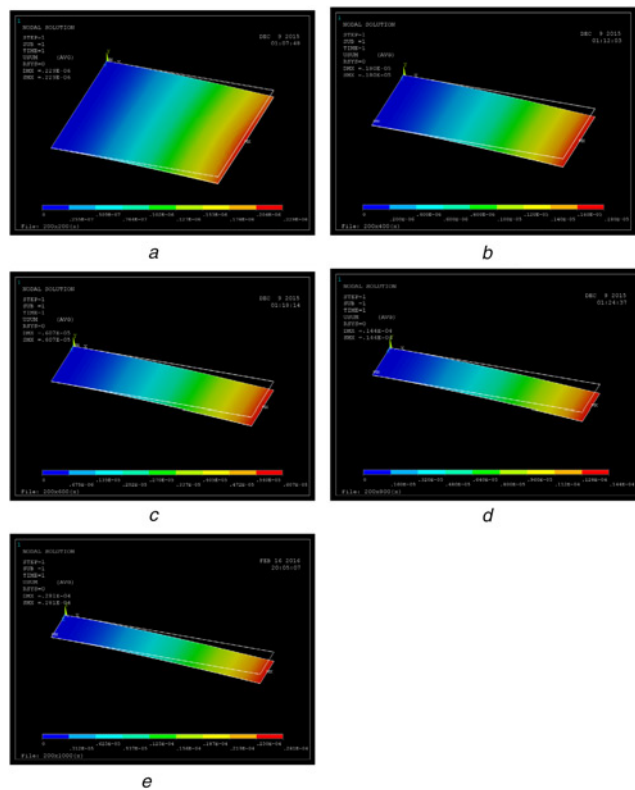


Fig. 3 Simulated deflection of type 1 cantilever beam at a width of 200 μm and various lengths when a force of 200 μN was exerted on the free end
a 200
b 400
c 600
d 800
e 1000 μm

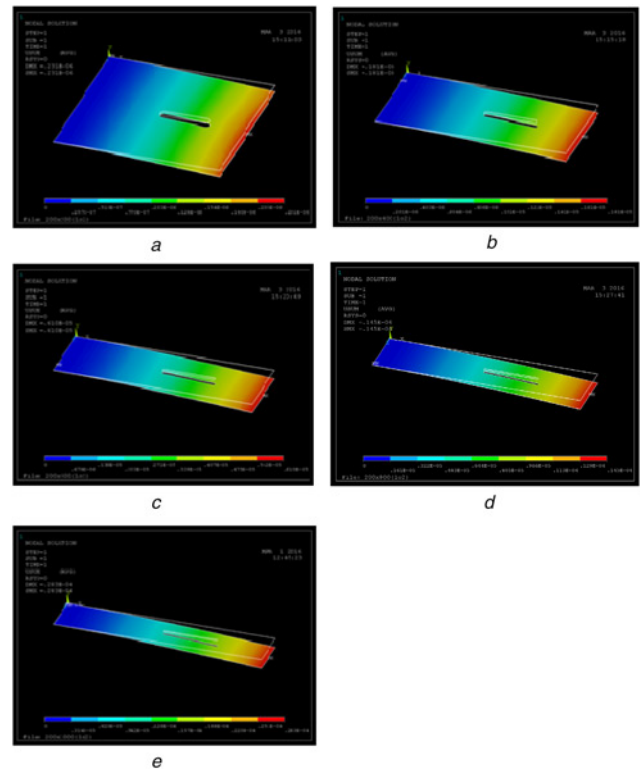


Fig. 4 Simulated deflection of type 2 cantilever beam at a width of 200 μm and various lengths when a force of 200 μN was exerted on the free end
a 200
b 400
c 600
d 800
e 1000 μm

maximum deflections of types 1–5 were 7.02, 7.11, 7.27, 7.71, and 7.35 μm , respectively. When the width was 200 μm , the maximum deflections of types 1–5 were 28.1, 28.3, 28.6, 29.4, and 28.7 μm , respectively. Compared with the cantilever beam without an etched slot, the cantilever beams with etched slots exhibited higher deflections; type 4 had the highest deflection, which increased by 4.6–22.3% for different widths and length-to-width ratios.

4.2. Appearances and sizes of cantilever beams after fabrication: Detailed images of the completed beams are presented in Figs. 7a–b. The sizes of the cantilever beams were based on the design requirement. The difference between the designed and actual sizes of the cantilever beams was less than 10%, and the difference between the designed and actual sizes of the etched slots was less than 20%. The success rate of the cantilever beam fabrication process is shown in Fig. 8. When the length of the type 1 cantilever beam was 400 μm or higher, the cantilever beam would easily collapse due to capillary force, and the success rate of the fabrication process was lower than 50%. When an etched slot was present, the lengths of the types 2–5 cantilever beams were 400 μm or higher, the phenomenon of collapse improved, and the success rate of the fabrication process was higher than 70%. The success rate of fabricating the type 4 beam was the highest and could be 85% when at lengths of 400 μm or higher. The important reason of microcantilever beams fabrication failure is the capillary force when the drying process, it results in that the base of the microcantilever beam was broken easily. The etched slots can decrease the capillary force, and the etched slot near the base of the cantilever beam was efficient. The etched slot of type 4 was near the base of the cantilever beam, and the success rate was the highest.

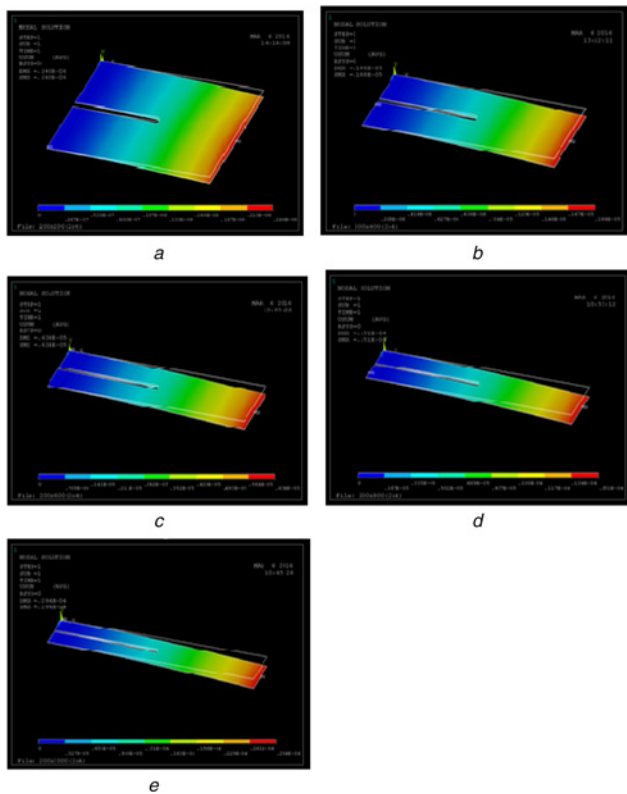


Fig. 5 Simulated deflection of type 4 cantilever beam at a width of 200 μm and various lengths when a force of 200 μN was exerted on the free end
a 200
b 400
c 600
d 800
e 1000 μm

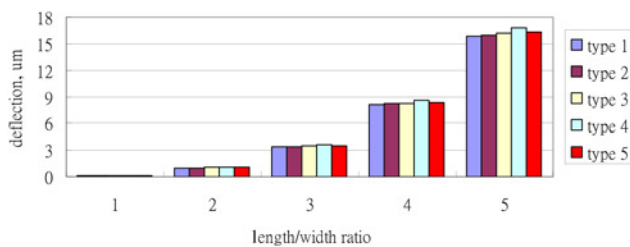


Fig. 6 Simulated deflections of various types and length-to-width ratios with width
a 50
b 100
c 150
d 200 μm

4.3. Comparison of etching time at various designs: To understand the etching time of the cantilever beams of various types, the lengths of the cantilever beams were measured and recorded every hour when the etching time was shorter than 3 h. When the etching time was longer than 3 h, the lengths of the cantilever beams were measured and recorded every 30 min. The etched slots of the cantilever beams could increase the etching area, and the etching time could be decreased. The etching time of the various types of cantilever beams is shown in Figs. 9a–c. The experimental data demonstrated that the etched slots were useful for reducing the etching time of the cantilever beams whose lengths were 300 μm or longer. The etched slots of the cantilever beams could increase the etching area, and the etching time could be decreased. The areas of the etched slots of types 4 and 5 were

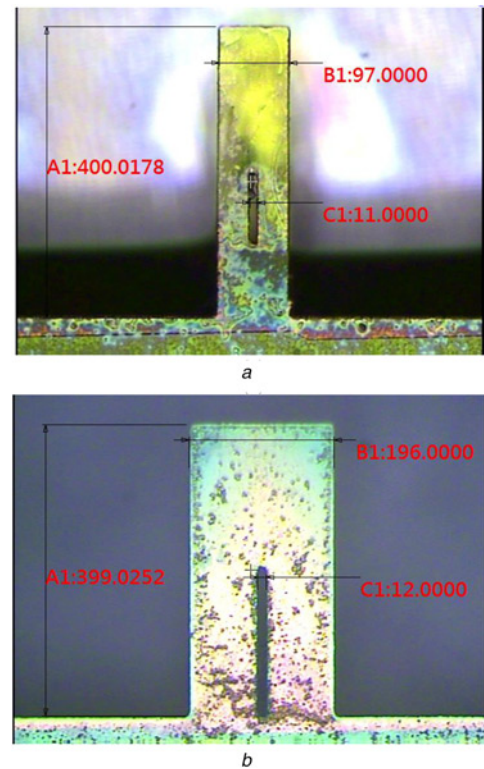


Fig. 7 Image of the completed cantilever beams with widths of
a 100
b 200 μm

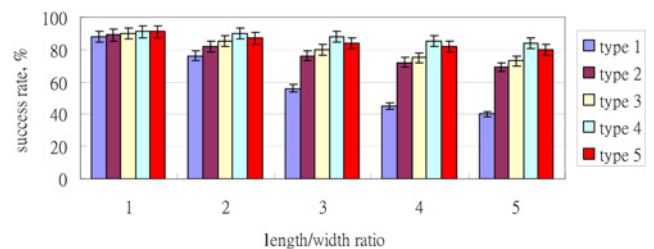


Fig. 8 Success rate of the fabrication of various types of cantilever beams with a width of 100 μm and various length-to-width ratios

larger, and the etching time was observed to be shorter. The etched slot of type 4 was near the base of the cantilever beam, and the etching time was observed to be the shortest. This structure conserved 1–3 h of fabrication time. Therefore, the etched slots were particularly useful for reducing the etching time for the fabrication of long cantilever beams.

4.4. Parameters modifications: Owing to the instrument limitations of the nanoindenter, the actual force acting point was on the $L/8$ location near the free end, not on the free end, in the experiment conducted using the nanoindentation technique; L is the total length of the cantilever beam. By contrast, the force acting point was on the free end in the simulation. This caused differences between the experimental and simulation results. A nanoindenter was also used to measure Young's modulus. For convenience, it is usual that one used the databases of the software. However, Young's moduli are in a large range [38], before Young's modulus of a sample was measured, the actual value could not be determined directly and easily. The value of Young's modulus of silicon nitride in ANSYS was determined to be 142 GPa, but the measured value E was 120 GPa (E_r was 115.1 GPa), yielding a

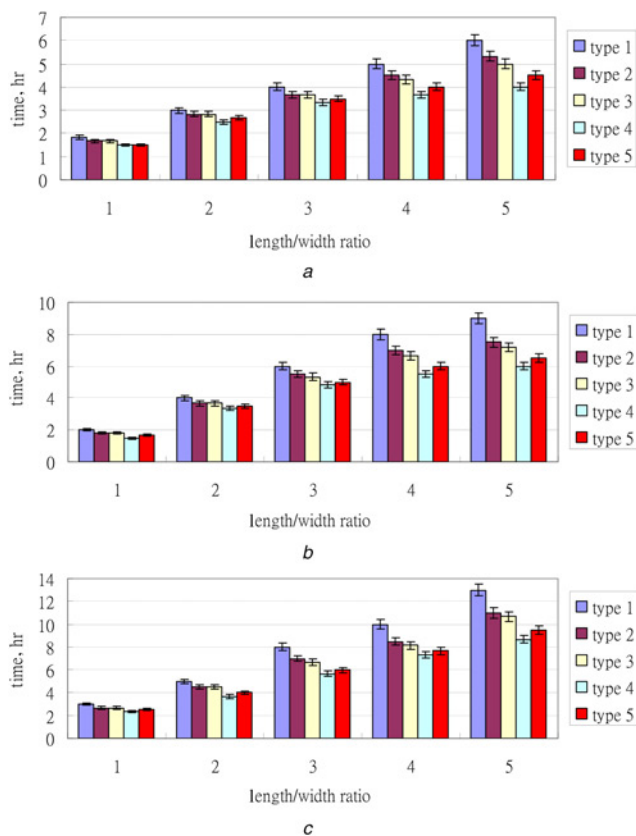


Fig. 9 Etching time of cantilever beams of various types and widths
a 100
b 150
c 200 μm

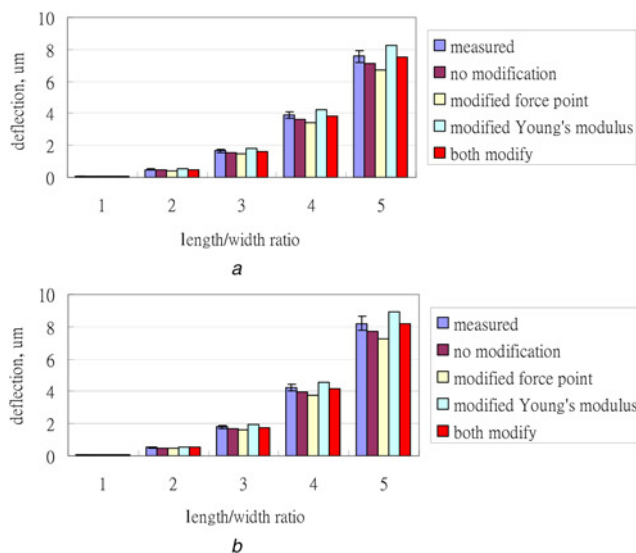


Fig. 10 Deflection comparison of the measurement and simulation with or without parameter modification for
a type 2
b type 4 beams

difference of 15.7%; therefore, the parameter required modification. If the Poisson's ratio of the Si_3N_4 material (0.27) in ANSYS software was used. The Young's modulus, based on this value (0.27), would be 118.6 GPa. The difference was 1.16%. The measured and simulated deflections for types 2 and 4 were compared, and the results are shown in Figs. 10a and b. In Figs. 10a and b,

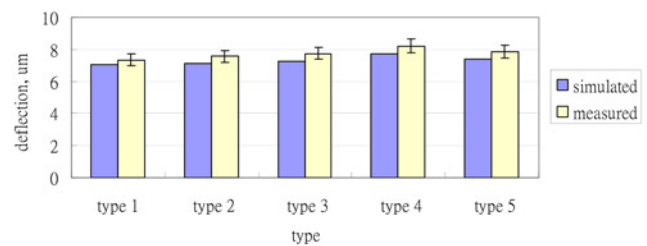


Fig. 11 Deflections obtained from the measurement and simulation without parameter modification for various types of cantilever beams with a width of 100 μm and length of 500 μm

the first column was the measured value, and the other four columns were the simulated values. In type 2, the measured deflection was greater than the simulated deflection – as determined without modification of the force acting point or Young's modulus – yielding a difference of 6.2%. When only the force acting point was modified (from the free end to the $L/8$ location near the free end), the measured deflection was greater than the simulated deflection, yielding a difference of 12.9%. When only Young's modulus was modified (142 GPa was corrected to 120 GPa), the measured deflection was smaller than the simulated deflection, yielding a difference of 8.5%. When both the force acting point and Young's modulus were modified, the measured deflection was slightly greater than the simulated deflection, yielding a difference of only 0.5%. As illustrated in Fig. 10b, the deflection variations of type 4 were similar to those of type 2, and the difference in the percentages were slightly lower. The comparison of the measured and simulated deflections demonstrates the importance of using simulated parameters that sufficiently match actual values; thus, the difference between the simulated and measured results can be negligible. The measured and simulated deflections without modification of the five types of cantilever beams with a width of 100 μm and length of 500 μm are shown in Fig. 11. The measured deflections were slightly greater than the simulated deflections. The deflections of the cantilever beam with an etched slot were greater than that of the cantilever beam without an etched slot. The deflection of type 4 was the greatest, and the deflections of types 1 and 4 differed by more than 10%. A cantilever beam with an etched slot can increase the corresponding deflection.

5. Conclusions: We propose a method for microcantilever beam fabrication that entails the use of an etched slot to reduce the etching time. The method was successfully applied to silicon nitride-based microcantilever beam fabrication. The deflection and force relationship in cantilever beams of various types were simulated using ANSYS software. The experimental and simulation results reveal that a microcantilever beam with an etched slot could reduce the etching time during fabrication, increase the success rate of the fabrication process, and increase the deflection of the cantilever beam. Moreover, the etching time was considerably reduced when the cantilever beam length was 300 μm or higher. The etching time of the type 4 beam was the shortest, and 1–3 h could be conserved during fabrication. The success rate of fabricating the type 4 beam was the highest (85%). The deflection of the type 4 beam was also the highest. Moreover, the deflections of the cantilever beams with and without an etched slot differed by more than 4.6%. Using the appropriate Young's modulus and force acting point was revealed to considerably influence the simulated deflection. Specifically, when the measured Young's modulus and actual force acting point were used, the difference between the simulated and measured deflections decreased to 0.5%. Therefore, the use of appropriate boundary conditions and parameters of the materials are important in simulation processes. The advantages

of the cantilever beam with etched slots were shorter fabricating time, larger deflection, and higher success rate of fabrication.

6 References

- [1] Liu J., Zhu X., Li X., *ET AL.*: 'Abnormal bending of micro-cantilever plate induced by a droplet', *Acta Mech. Solida Sin.*, 2010, **23**, pp. 428–436
- [2] Zhuang F.K., Tu S.T., Zhou G.Y., *ET AL.*: 'A small cantilever beam test for determination of creep properties of materials', *Fatigue Fract. Eng. Mater. Struct.*, 2015, **38**, pp. 257–267
- [3] Hopcroft M., Kramer T., Kim G., *ET AL.*: 'Micromechanical testing of SU-8 cantilevers', *Fatigue Fract. Eng. Mater. Struct.*, 2005, **28**, pp. 735–742
- [4] Snow D., Weeks L.B., Kim D.J., *ET AL.*: 'Static deflection measurements of cantilever arrays reveal polymer film expansion and contraction', *J. Colloid Interface Sci.*, 2007, **316**, pp. 687–693
- [5] Arya S., Khan S., Lehana P.: 'Design and fabrication of electrostatic micro-cantilever array as audible frequency generator', *J. Electrostat.*, 2015, **76**, pp. 145–151
- [6] Komeili M., Menon C.: 'Modelling a micro-cantilever vibrating in vacuum, gas or liquid under thermal base excitation', *Mech. Res. Commun.*, 2016, **73**, pp. 39–46
- [7] Zhou L., Giri A., Cho K., *ET AL.*: 'Mechanical anomaly observed in Ni-Mn-Ga alloys by nanoindentation', *Acta Mater.*, 2016, **118**, pp. 54–63
- [8] Hu Z., Shrestha M., Fan Q.H.: 'Nanomechanical characterization of porous anodic aluminum oxide films by nanoindentation', *Thin Solid Films*, 2016, **598**, pp. 131–140
- [9] He B.B., Huang M.X., Liang Z.Y., *ET AL.*: 'Nanoindentation investigation on the mechanical stability of individual austenite grains in a medium-Mn transformation-induced plasticity steel', *Scr. Mater.*, 2013, **69**, pp. 215–218
- [10] Li M.C., Jiang M.Q., Jiang F., *ET AL.*: 'Testing effects on hardness of a Zr-based metallic glass under nanoindentation', *Scr. Mater.*, 2017, **138**, pp. 120–123
- [11] Liang W., Ning Z., Dang Z., *ET AL.*: 'Plastic deformation behaviors of Ni- and Zr-based bulk metallic glasses subjected to nanoindentation', *Mater. Charact.*, 2013, **86**, pp. 290–295
- [12] Zhang Z., Zhang N., Ma G., *ET AL.*: 'Characterization of microstructural stability for nanotwinned mercury cadmium telluride under cyclic nanoindentations', *Scr. Mater.*, 2013, **69**, pp. 299–302
- [13] Concustell A., Mattern N., Wendrock H., *ET AL.*: 'Mechanical properties of a two-phase amorphous Ni–Nb–Y alloy studied by nanoindentation', *Scr. Mater.*, 2007, **56**, pp. 85–88
- [14] Broitman E., Tengdelius L., Hangen U.D., *ET AL.*: 'High-temperature nanoindentation of epitaxial ZrB₂ thin films', *Scr. Mater.*, 2016, **124**, pp. 117–120
- [15] Wang Y., Cheng Y.: 'A nanoindentation study of the viscoplastic behavior of pure lithium', *Scr. Mater.*, 2017, **130**, pp. 191–195
- [16] Moniruzzaman M., Zioupos P., Fernando G.F.: 'Investigation of reversible photo-mechanical properties of azobenzene-based polymer films by nanoindentation', *Scr. Mater.*, 2006, **54**, pp. 257–261
- [17] Hong Y., Zhou C., Zheng Y., *ET AL.*: 'Hydrogen effect on the deformation evolution process in situ detected by nanoindentation continuous stiffness measurement', *Mater. Charact.*, 2017, **127**, pp. 35–40
- [18] Charitidis C.A., Skarmoutsou A., Tsetsekou A., *ET AL.*: 'Nanomechanical properties of hydroxyapatite (HAP) with DAB dendrimers (poly-propylene imine) coatings onto titanium surfaces', *Mater. Sci. Eng., B*, 2013, **178**, pp. 391–399
- [19] Li X., Bhushan B.: 'A review of nanoindentation continuous stiffness measurement technique and its applications', *Mater. Charact.*, 2002, **48**, pp. 11–36
- [20] Su J.F., Wang X.Y., Dong H.: 'Micromechanical properties of melamine-formaldehyde microcapsules micromechanical properties of melamine-formaldehyde microcapsules', *Mater. Lett.*, 2012, **89**, pp. 1–4
- [21] Al-Halhouli A.T., Kampen I., Krah T., *ET AL.*: 'Nanoindentation testing of SU-8 photoresist mechanical properties', *Microelectron. Eng.*, 2008, **85**, pp. 942–944
- [22] Zhang Q., Gao S., Min J., *ET AL.*: 'Graded viscoelastic behavior of human enamel by nanoindentation', *Mater. Lett.*, 2016, **179**, pp. 126–129
- [23] Tanguy M., Bourmaud A., Baley C.: 'Plant cell walls to reinforce composite materials: relationship between nanoindentation and tensile modulus', *Mater. Lett.*, 2016, **167**, pp. 161–164
- [24] Singh S.S., Jansen M.A., Franz N., *ET AL.*: 'Microstructure and nanoindentation of the rostrum of *Curculio longinasus* Chittenden, 1927 (Coleoptera: Curculionidae)', *Mater. Charact.*, 2016, **118**, pp. 206–211
- [25] Kim Y.Y.: 'Young's modulus measurement of a silicon nitride thin-film using an ultrasonically actuated microcantilever', *Measurement*, 2018, **115**, pp. 133–138
- [26] Petersen K.E.: 'Dynamic micromechanics on silicon: techniques and devices', *IEEE Trans. Electron Devices*, 1978, **25**, pp. 1241–1250
- [27] Roylance L.M., Angell J.B.: 'A batch-fabricated silicon accelerometer', *IEEE Trans. Electron Devices*, 1979, **26**, pp. 1911–1917
- [28] Barnes J.R., Stephenson R.J., Welland M.E., *ET AL.*: 'Photothermal spectroscopy with femtojoule sensitivity using a micromechanical device', *Nature*, 1994, **372**, pp. 79–81
- [29] Oden P.I., Chen G.Y., Steele R.A., *ET AL.*: 'Viscous drag measurements utilizing microfabricated cantilevers', *Appl. Phys. Lett.*, 1996, **68**, pp. 3814–3816
- [30] Arakawa E.T., Lavrik N.V., Rajiv S., *ET AL.*: 'Detection and differentiation of biological species using microcalorimetric spectroscopy', *Ultramicroscopy*, 2003, **97**, pp. 459–465
- [31] Battison F.M., Ramseyer J.P., Lang H.P., *ET AL.*: 'A chemical sensor based on a microfabricated cantilever array with simultaneous resonance-frequency and bending readout', *Sens. Actuators B*, 2001, **77**, pp. 122–131
- [32] Lee J.H., Hwang K.S., Park J., *ET AL.*: 'Immunoassay of prostate-specific antigen (PSA) using resonant frequency shift of piezoelectric nanomechanical microcantilever', *Biosens. Bioelectron.*, 2005, **20**, pp. 2157–2162
- [33] Ilic B., Yang Y., Aubin K., *ET AL.*: 'Enumeration of DNA molecules bound to a nanomechanical oscillator', *Nanoletters*, 2005, **5**, pp. 925–929
- [34] Wu G.H., Datar R.H., Hansen K.M., *ET AL.*: 'Bioassay of prostate-specific antigen (PSA) using microcantilever', *Nat. Biotechnol.*, 2001, **19**, pp. 856–860
- [35] Hibbeler R.C.: 'Mechanics of materials' (Pearson Education, UK, 2016, 10th edn.)
- [36] Oliver W.C., Pharr G.M.: 'An improved technique for determining hardness and elastic modulus using load and displacement sensing indentation experiments', *J. Mater. Res.*, 1992, **7**, pp. 1564–1583
- [37] Wang P.C., Lee J.W., Yang T.C., *ET AL.*: 'Effects of silicon contents on the characteristics of Zr-Ti-Si-W thin film metallic glasses', *Thin Solid Films*, 2016, **618**, pp. 28–35
- [38] Kim Y.Y.: 'Young's modulus measurement of a silicon nitride thin-film using an ultrasonically actuated microcantilever', *Measurement*, 2018, **115**, pp. 133–138